Supplementary Information for Optospintronics in Graphene *via* Proximity Coupling

Ahmet Avsar,[1*+] Dmitrii Unuchek,[1+] Jiawei Liu,[2] Oriol Lopez Sanchez,[1] Kenji Watanabe,[3] Takashi Taniguchi,[3] Barbaros Özyilmaz,[2] Andras Kis[1*]

[1] Electrical Engineering Institute and Institute of Materials Science and Engineering, École Polytechnique Fédérale de Lausanne (EPFL), Lausanne CH 1015, Switzerland.

[2] Centre for Advanced 2D Materials, National University of Singapore, Singapore 117542, Singapore.

[3] National Institute for Materials Science, 1-1 Namiki, Tsukuba 305-0044, Japan

S1. Half wave (λ/4) modulation by PEM

In the case of λ/2 modulation, applied retardation has maximal (minimal) value of λ/2 (-λ/2) with PEM acting as a half wave plate at these moments, thus rotating the incident polarization by 2θ (90° in the case of 45° incidence), preserving its linearity. Lock-in amplification of the sample electrical response with the reference signal (gray dashed line) at double the PEM operating frequency (100kHz, 2f) results in a signal that corresponds to the variation in the non-local signal caused by the original and rotated linearly polarized light. Here, the resulting light modulation is linear to linear. The corresponding device set-up is shown in fig.S1.
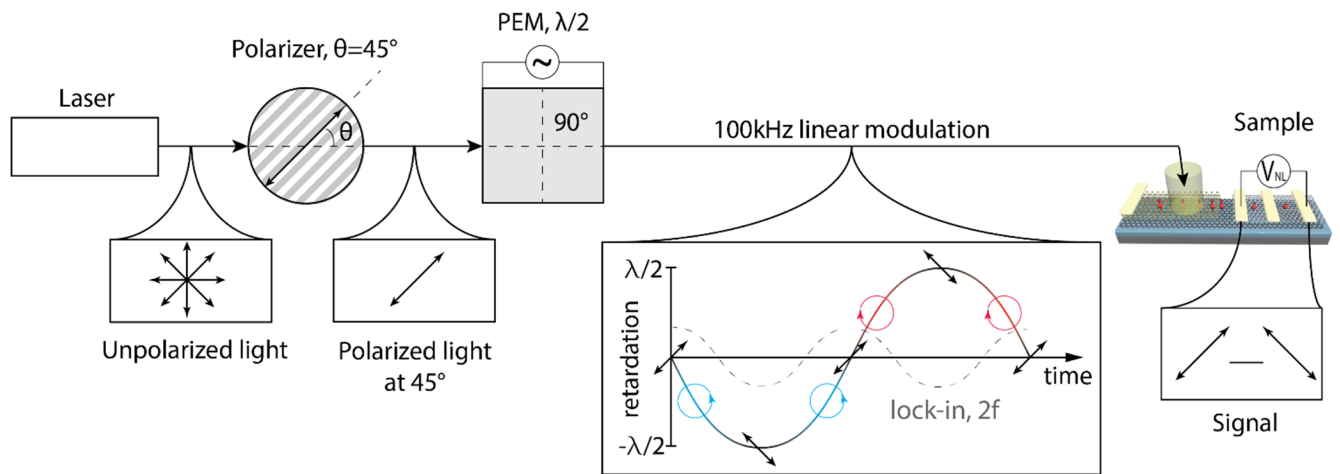

Figure S1. Schematics of the experimental set-up for achieving half wave modulation. Measurement schematics for achieving half wave modulation and electrical detection of non-local signal.

S2. Light modulation dependence on the polarization angle rotation

The sketch shown in fig. S2. represents schematic results of light modulation for three particular angles of incidence (θ = 45°, 22°, 0° from the top to the bottom) in the cases of quarter wave and half wave modulation (left and right parts respectively). Since the PEM operated in a λ/4 mode acts as a time-dependent quarter wave plate, it results in the modulation of the circular handedness of the light if

incident at 45° angle to the PEM axis (upper left drawing). Deviating θ from the 45° angle, results in the components of light parallel and perpendicular to the PEM optical axis being taken out of balance, thereby increasing ellipticity of the modulated light (middle left). Light incident at θ = 0° (bottom left schematic) is not influenced by the PEM since it is oriented along its optical axis while only the component across this axis gets retarded. In other words, angle θ has a direct impact on the ellipticity degree of the light modulated by PEM operating in λ/4 mode and thus on the signal amplified by the lock-in. On the other hand, half-wave modulation (right part) is fundamentally different from the former case, since light is modulated linearly between θ and – θ at twice the frequency of PEM operation.
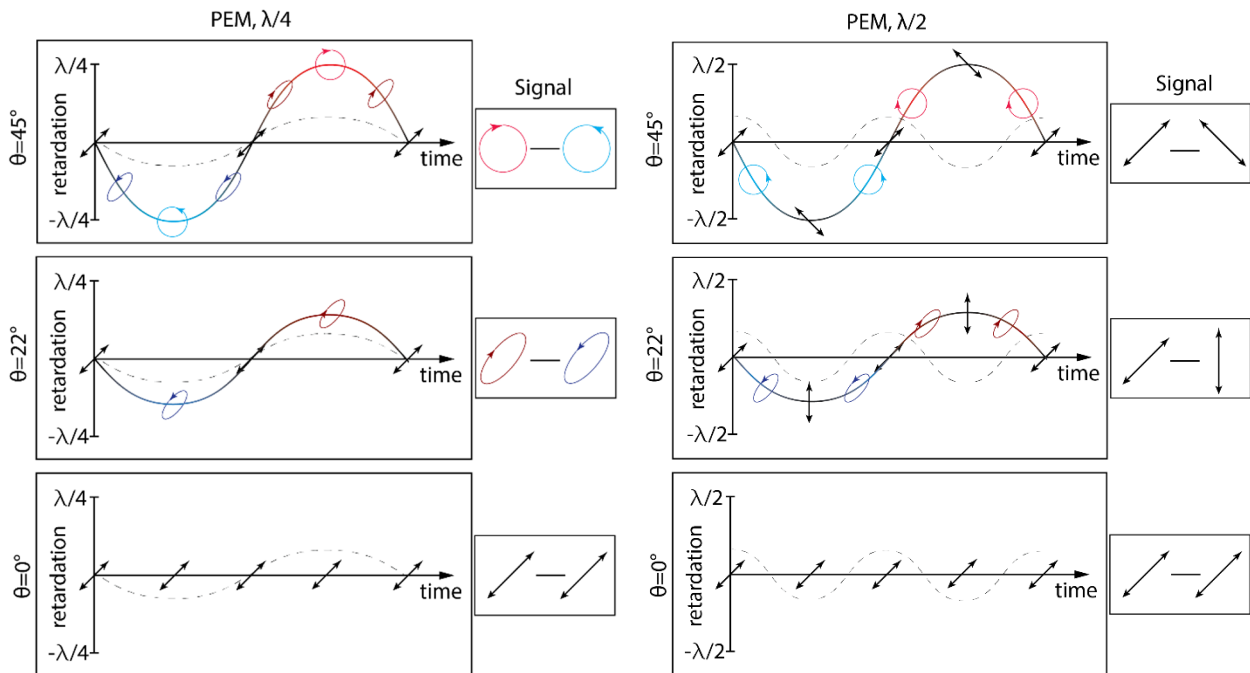

Figure S2. Schematics of the experimental set-up for achieving polarization angle rotation. Measurement schematics for achieving light modulation for three particular angles of incidence (θ = 45°, 22°, 0° from the top to the bottom) in the cases of quarter wave and half wave modulation (left and right parts respectively).

S3. Gate voltage dependence of extracted spin transport properties

In this section, we study the gate voltage dependence of spin transport in graphene. For this, we perform spin precession measurements under both parallel and anti-parallel polarization configurations and we extract spin transport parameters as described in the main text. We observe that extracted spin relaxation time, spin diffusion constant and spin relaxation length values are maximum near the charge neutrality point and decreases as we increases the carrier concentration. The maximum extracted spin relaxation time (length) value is ~ 225 ps (6.1 µm). The gate voltage dependence and the amplitude of these spin transport parameters are in a good agreement with what has been measured previously.
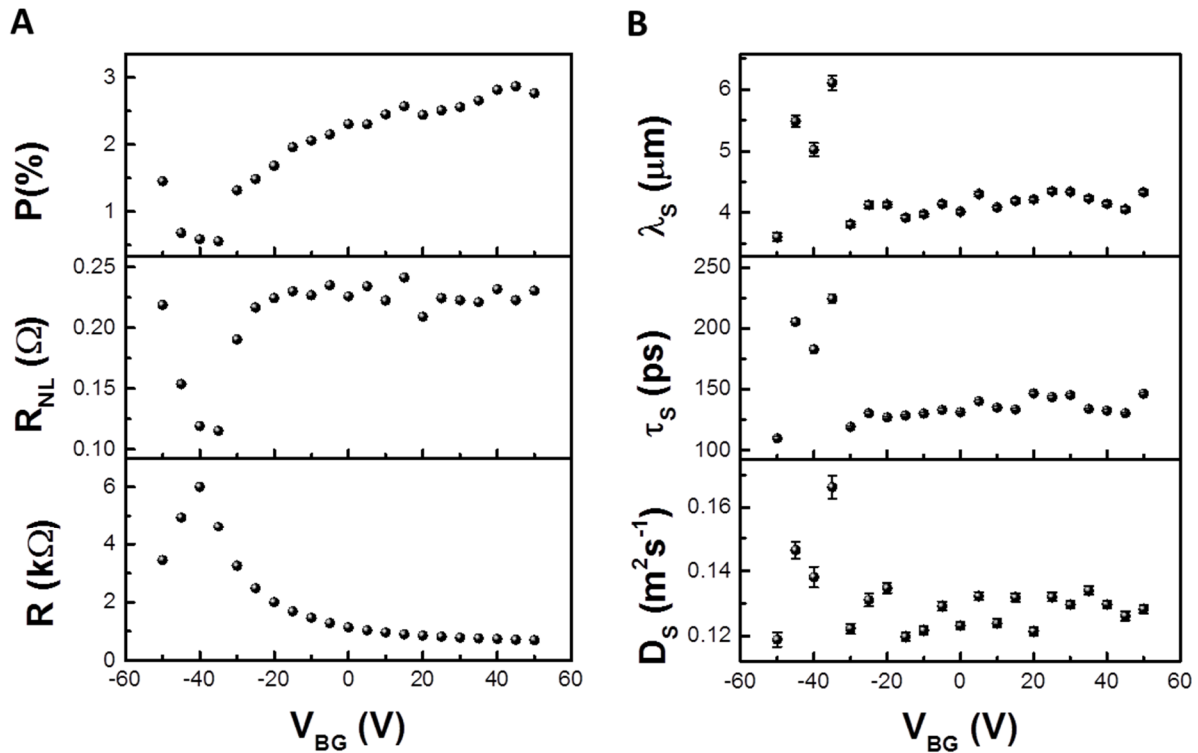

Figure S3. Gate voltage dependence of *P*, *R$_{NL}$*, *R*, *λ$_S$*, *τ$_S$*, *D$_S$*. **(A)** Back gate voltage (V$_{BG}$) dependences of spin polarization (*P*), non-local resistance (*R$_{NL}$*) and local resistance (*R*). **(B)** V$_{BG}$ dependences of spin relaxation length (*λ$_S$*), spin relaxation time (*τ$_S$*) and spin diffusion constant (*D$_S$*).

S4. Photoluminescence spectra of WSe$_2$

In order to confirm the monolayer thickness of our WSe$_2$ layer, we measure the photoluminescence spectrum (fig. S4). Blue curve represents the PL spectrum obtained at the center of the WSe$_2$ monolayer, while red curve shows PL from the more defective edge of the flake. In the center of the monolayer, the excitonic emission is dominant (1.66 eV, X^0). In contrast, higher density of defects as well as the presence of bilayer in the edge area results in stronger recombination of the localized electrons leading appearance of well-pronounced low energy peak (1.58 eV, X'). Insert shows the optical image of the device with indicated locations of PL measurements. All PL spectra were obtained at 488 nm excitation wavelength with 40 µW incident power. Measurements were performed at 4K.
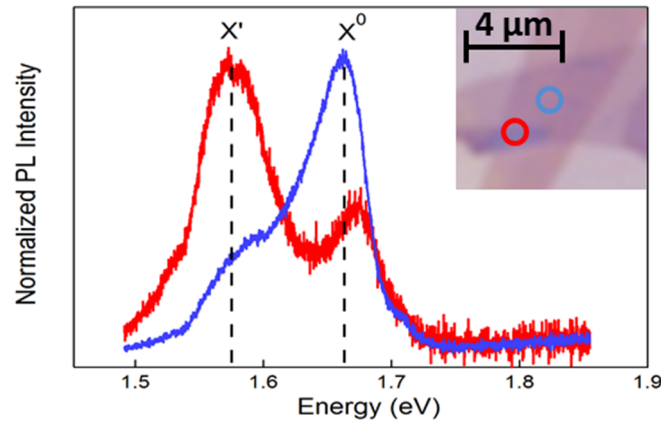

Figure S4. Normalized photoluminescence spectra of WSe$_2$. Energy dependence of the normalized PL intensity for mono and multilayer of WSe$_2$. Blue curve represents the PL spectrum obtained at the center of the WSe$_2$ monolayer. Red curve shows PL from the more defective edge of the flake.

S5. Spot location dependence of non-local signal

We move the incident light spot across the heterostructure as the non-local voltage is recorded for the case of λ/4 modulation. Excitation wavelength is 720 nm and incident power is 180 µW. Red arrow in fig. S5. shows the direction of motion. We see an enhanced signal once the spot is on the WSe$_2$/graphene heterostructure. We note that the signal is slightly location dependent which could be related with

interface quality between graphene and WSe$_2$. As expected, the signal disappears if the spot is parked on graphene. Measurements were performed at 4K.
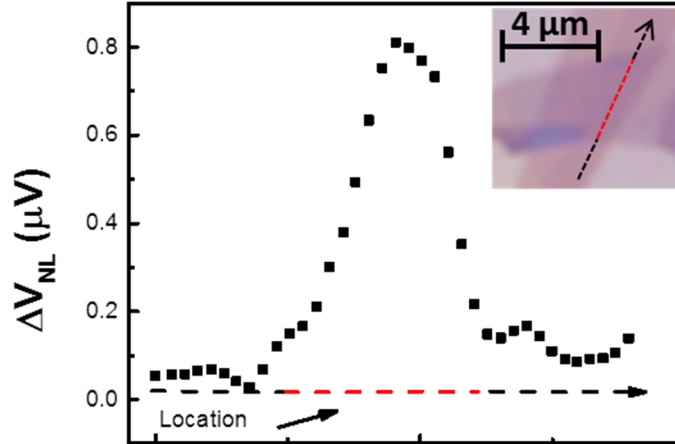

Figure S5. Location dependence on the non-local signal. Inset shows the optical image of the heterostructure device. As we move the incident light spot across the heterostructure (arrow direction), the non-local voltage is simultaneously detected for the case of $\lambda/4$ modulation. We see an enhanced signal only once the spot is on the WSe$_2$/graphene interface.

S6. Incident angle dependences of non-local signal for $\lambda/2$ and $\lambda/4$ modulations

Non-local signal as a function of the incident light angle θ at half-wave modulation (red dots) and quarter-wave modulation (blue dots) are studied (fig. S6). Black solid line shows sine function of twice the angle of incidence (2θ) as a representation of the ellipticity degree of the modulated light. While we observe strong incident angle dependences of non-local signal for $\lambda/4$ modulation, it is absent for $\lambda/2$ modulation case which proves the opto-valleytronic origin of spin injection process.
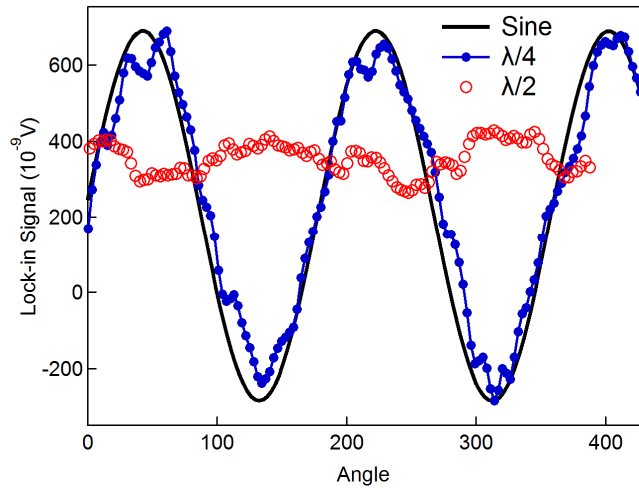
Figure S6. Spin signal dependence on the ellipticity degree. Non-local signal as a function of the incident light angle θ at half-wave modulation (red dots) and quarter-wave modulation (blue dots). We see high non-local signal and ellipticity dependence only for quarter-wave modulation.